A Fluid Dynamics Approach to Planetesimal Formation

John McNamara

Readers: David Bercovici and Jun Korenga

May 5, 2017

A Senior Thesis presented to the faculty of the Department of Geology and Geophysics, Yale University, in partial fulfillment of the Bachelor's Degree.

Abstract

The core accretion model—the most widely accepted theory of solar system formation—posits that planets begins their life cycles as microscopic dust particles orbiting young star through a gaseous disk. According to this theory, as the dust particles move through the gas, they collide and adhere, eventually forming kilometer-sized bodies known as planetesimals [Lissauer (1993)]. However, there are many processes in planet formation, such as overcoming the one-meter hurdle and the processes of planetary migration, that this hypothesis does not explain. As such, astrophysicists have developed several alternate hypotheses for planet formation, most notably the gravitational instability and streaming instability hypotheses [Youdin and Goodman (2005)].

In this paper, I examine a simple model of protoplanetary disks, treating an early solar system as an inviscid gas disk with azimuthal symmetry. Dust within the disk is phase-locked with the gas, and density (ρ) and temperature (T) within the disk obey a power laws with respect to the distance from the central star (r). I assume a background steady state of zero radial velocity and a sub-Keplerian angular velocity. I then apply linear perturbation analysis to this system's non-dimensionalized equations for conservation of fluid mass and momentum. I find that perturbations to radial velocity exhibit oscillatory behavior; and for $T \propto r^-1$, these oscillations are a Bessel function in $\frac{2\omega r^{3/2}}{3}$ where ω is the perturbation frequency. The order of the Bessel function is determined by α, the ratio of the Keplerian velocity to the gas sound speed at a reference radius $r = r_0$. I then examine how these oscillations change with varying values of n, m, and α as well as how these waves could potentially offer remedies to the one-meter hurdle and planetary migration.

Background and Motivation

Scientific theories about the origin of the universe are nearly as old as human civilization itself, as great thinkers throughout history have speculated on the origins of planets, stars, and other celestial bodies. However, nearly all of these speculations were based exclusively on observations about our solar system, since that was the only data available for most of human history. It has only been within the last two decades with the discovery of extra-solar planets [Mayor and Queloz (1995)] that we have been able to observe additional planets outside our solar system. Many of the newly discovered systems have properties that are vastly different from ours, such

as Pegasi 51-b, a massive gas giant planet with an orbital period of just four days [Mayor and Queloz (1995)], the Kepler-11 system, which contains five planets all with semi-major axes shorter than Mercury's [Lissauer et al. (2011)], and the Kepler-16 system, which harbors a "modern Tatooine" orbiting a binary star system [Doyle et al. (2011)]. However, despite these systems' vastly different features, the underlying physics governing formation and subsequent evolution of all solar systems must be the same. As a result, many old assumptions and theories about how planets form need to be reevaluated, or at the very least modified, in order to account for these new observations. This need has led to a plethora of proposals of new mechanisms and theories in recent years, of which some of the most important and notable are outlined below.

The Core Accretion Model

The most popular and widely accepted theory is still the one developed before the discovery of exoplanets, the steady accretion, or core accretion model. Although exoplanet discoveries have resulted in minor modifications to this theory, the modern understanding of the model is similar to its earliest forms [Safronov (1972), Hayashi et al. (1985), Lissauer (1993)]. Solar systems begin as rotating clouds of gas (primarily H and He) and dust (solid ice, rock, or metal particles) rotating about a young star [Watson et al. (2007)]. Eventually, the centripetal acceleration of this cloud causes all of the material to collapse into a disk Chiang and Youdin (2010) Lin (2008). The primary forces governing the orbits of solid particles (dust grains) is simply the balance between centripetal acceleration and the gravity of the central star. This causes the dust particles to orbit at the Keplerian velocity ($v_k = \sqrt{\frac{GM}{r}}$ where M is the star's mass.) However, gas, which comprises 99% of the material within the disk [Chiang and Youdin (2010)], has a different force balance. Because gas is a fluid, it experiences a pressure gradient force that partially counteracts the gravitational attraction from the central star. This additional force causes the gas to orbit at a sub-Keplerian velocity

$$v = \sqrt{v_k^2 - \eta} \tag{1}$$

where $\eta \equiv -\frac{1}{\rho}\frac{\partial P}{\partial r}$ [Armitage (2010)].

This velocity difference causes large dust grains to experience a significant drag force as they orbit, which causes them to lose angular momentum and spiral inward toward the central

Figure 1: Illustration showing the earliest stages of planetesimal growth. Dust particles collide, are swept up by the gas, and accumulate at the snow line. Source: Lin (2008)

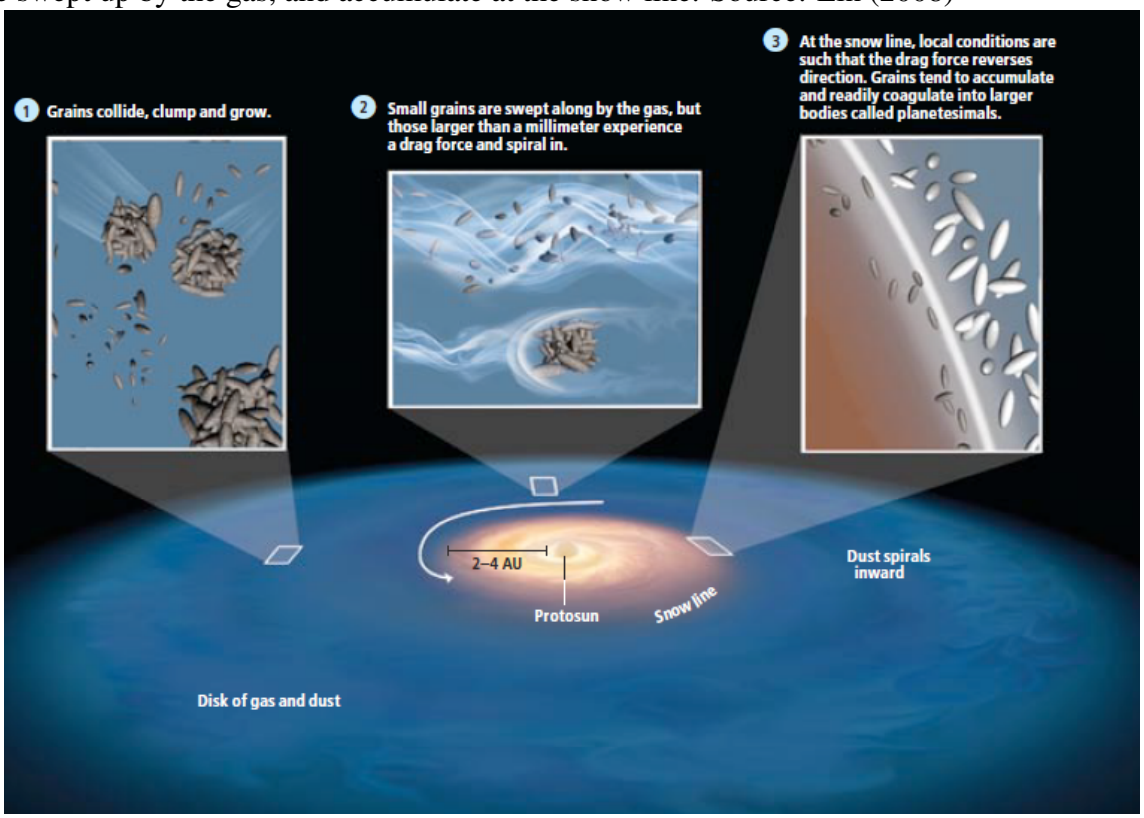

star [Lin (2008)]. As the grains travel through the disk, they occasionally collide with one another, and if conditions are suitable, a collision can cause two particles to stick together, forming a larger particle [Blum and Wurm (2008)]. Although these collisions can occur anywhere within the disk, they are most common at local pressure maxima, where dust particles tend to accumulate. One such maximum is the point at which it becomes warm enough for volatiles such as water to boil off from dust grains, a region approximately 2-4 AU from the central star known as the "snow line." Furthermore, collisions near the snow line are also more likely to build up grain size, since the boiled-off volatiles make the grains more "sticky" and more likely to adhere upon collision. Eventually through such collisions, these particles grow from micron-sized to dust grains to massive, kilometer-sized bodies known as "planetesimals", the building blocks of planets [Lissauer (1993)].

Collisions between solid bodies in the early solar system remain common even after they reach planetesimal-size, and these collisions result in a distribution of planetesimal masses. The largest planetesimals are massive enough to draw in nearby material due to gravity. Initially this leads to even more growth, but eventually, the planetesimal will "consume" all of the nearby material, and become so massive that it deflects the orbits of nearby particles rather

than drawing them in. As a result, after about one millions years, most of the solid material in the proto-planetary disk becomes concentrated within an "oligarchy" of planetary embryos with massses ranging from that of the moon in the inner solar system to several times that of Earth in the outer solar system [Lissauer (1993)].

At this stage of development, sufficiently massive planetary embryos ($\sim$10 Earth masses) will have a strong enough gravitational potential to draw in nearby gas. However, in order for this accumulation to result in a full-fledged planet, the gas accumulation rate must dominate over the rates of both gas depletion due to stellar winds and planetary migration (a process discussed in detail below). Since all three of these processes occur over similar timescales, ultimately which embryos grow into planets is all down to luck. However, for embryos in which growth by gas accumulation dominates, the transition from embryo to planet occurs surprisingly quickly; an embryo can grow to a planet with one-half Jupiter mass in roughly 1000 years. Eventually, the planet becomes massive enough to significantly alter the flow of the neighboring gas. The new planet's gravity causes gas interior to the planet's orbit to orbit more quickly, while gas exterior to the planet orbits more slowly. Both of these processes cause gas to move away from the planet, stabilizing its orbit and clearing out a region of the disk devoid of gas [Lin (2008)].

This clearing of gas along the new planet's orbit disrupts the pressure profile of the disk, creating new regions of local pressure maxima. As a result, the presence of one gas giant can spark renewed plantesimal growth, which can in turn lead to the development of additional gas giant [de Val-Borro et al. (2007)]. Many scientists believe that this is what happened in our solar system, with Jupiter begin directly responsible for the formation of Saturn, Uranus, and Neptune [Lin (2008)]. Gas giants must form within the first 10 million years of the solar-system's lifecycle, before all of the gas in the gas is blown away due to photoevaporation [Armitage (2011), Raymond (2007)]. Terrestrial planets, on the other hand, can take much longer to form. Planetary embryos in the inner solar system can continue to destabilze each other's orbits long after the gas from the disk has dissipated due to gravitational interactions with each other or with a distant gas giant, resulting in massive, cataclysmic collisions. The remnants of these collisions then coalesce into a larger body until, after tens of millions of years, the terrestrial planet's orbits stablize and the planet-formation process is complete [Raymond (2007)].

While the core-accretion model presents a plausible theory of planet formation and ad-

equately explains the sizes and orbits of the planets in our solar system, it is not without its problems. One of the most important and troubling problems with core-accretion deals with the earliest stages of planet development, when microscopic dust grains are developing into macroscopic bodies. When the dust particles are on the order of $1\mu m$ in diameter, they are essentially phase-locked to the gas and orbit at the sub-keplerian velocity described in equation (1). Additionally, planetesimal-sized bodies are essentially unaffected by gas drag, and orbit the central star at Keplerian velocities. However, drag becomes important once a particle grows beyond 1mm in diameter, as the gas drag will cause these bodies to lose angular momentum and spiral inward toward the center of the star. The timescales over which these particles will crash into the central star is incredibly short ($\propto 10^3$ years) relative to other processes in a proto-planetary disk, so these particles must grow incredibly quickly in order to avoid this fate [Blum and Wurm (2008)].

However, it is nearly impossible for particles to grow to planetesimal-sizes through collisions alone. A collision between two dust particles results in sticking if the relative velocity between the particles (v_{col}) is less than a critical velocity (v_{crit}). This critical velocity decreases with increasing particle size s; Chokshi et al. (1993) showed that $v_{crit} \propto s^{-5/6}$. By the time the particles reach 1cm in size (the critical velocity is an order of magnitude less than observed sticking velocities [Blum and Wurm (2008)]. As a result, solid particles cannot grow large enough fast enough to avoid falling into the central star, a problem known as the "one-meter-hurdle" [Youdin and Johansen (2007)]. If planetesimals form as a result of collisions, there must be some process at play that lowers the critical velocity. One hypothesis is that volatiles near the snow line make particles "stickier," enabling them to coalesce at higher collision velocities [Lin (2008)]. Another theory posits incorporating particle porosity can reduce the critical velocity. Despite these hypotheses, experimental results reveal that it is incredibly difficult to grow particles through collisions alone [Blum and Wurm (2008)], leading astrophysicists to search for another explanation.

However, assuming that one could find a solution to the one-meter hurdle, there remain additional problems to the core accretion model in the later stages of planet development. Planetary embryos large enough to spawn gas giants can only form in the outter reaches of the solar system, at distances greater than 5AU [Lissauer (1993)]. However, the first exoplanets discovered were massive gas giants with incredibly short orbital periods [Mayor and Queloz (1995)]. If these planets formed in the outer regions of their protoplanetary disks, how did they get to the

inner reaches of their solar systems, and once there, what stabilized their orbits? This problem is known as planetary migration, and there are a few solutions that have been proposed. One possible mechanism is that planets can migrate inward in response to gravitational interactions with other solid bodies in a disk. If a planet ejects a nearby planetesimal farther outward into the solar system, then in order to conserve angular momentum throughout the interaction, the planet must move inward to compensate for the smaller body's angular momentum increase [Levison et al. (2007)]. Planetary migration can also occur through tidal interactions between the planet and the gas disk. This type of migration can take two forms, both of which operate over similar timescales ($10^5 - 10^6$ years). Type I migration, the mechanism relevant for smaller protoplanets, occurs due to the planet exerting torque on density waves within the disk. By contrast, type II migration is relevant for larger planets and takes place due to viscous transfer of angular momentum after a planet has cleared all of the gas out of its orbital path [Papaloizou and Terquem (2005)]. However, while the processes drving planetary migration are fairly well-developed, much less is understood about what stops planetary migration and prevents a young planet from crashing into its host star. It has been suggested that magnetic fields could induce turbulence within the disk to halt type I migration [Papaloizou and Terquem (2005)], and type II could stop if migration coincided with the outward dissipation of the gas [Trilling et al. (2002)]. However, these theories cannot account for the locations of all observed exoplanets, and as such, further investigation into planetary migration is crucial in order to fully understand solar system evolution.

Alternate Hypotheses

In an attempt to remedy problems such as the one-meter hurdle and planetary migration, astrophysicists have proposed several planet formation models. One of the most popular and influential of these theories is the gravitational instability (GI) model [Boss (1997)]. This instability arises when axisymmetric perturbations in density lead to an overdense annulus of width Δr. The increased self-gravity from this overdense region attracts more material to the annulus, which would increase the density further, leading to an instability [Goodman and Pindor (2000)]. The GI model treats solid dust particles as a self-gravitating, rotating fluid confined to the disk midplane. According to Toomre (1964) if the perturbations scale as $e^{i(k_r r+\omega t)}$ and

$k_r r \gg 1$then the dispersion relation for such a model is

$$\omega^2 = c^2 k_r^2 - 2\pi G\Sigma|k_r| + \kappa^2 \tag{2}$$

Here, c is the velocity dispersion, $\kappa \equiv (r\frac{\partial\Omega^2}{\partial r} + 4\Omega^2)^{1/2}$, Ω is the angular speed of the dust, Σ is the dust surface density, and G is the universal gravitational constant. This relation reveals that pressure from the fluid (the κ^2 term) stabilizes short-wavelength perturbations and rotation (the c^2k^2 term) stabilizes long-wave perturbations. However, the dust's self-gravity can destabilize perturbations of intermediate wavelengths Binney and Tremaine (2011) Chiang and Youdin (2010). These intermediate wavelengths are unstable if Toomre's criterion is met, which necessitates that

$$Q \equiv \frac{c\kappa}{\pi G\Sigma} < 1 \tag{3}$$

(3) can also be written as a thickness requirement for the dust layer; gravitational instabilities can only occur if the midplane layer depth h_p satisfies

$$h_p < h_p^* \approx 2 * 10^6 F Z_{rel} \left(\frac{r}{AU}\right)^{3/2} m \tag{4}$$

where F and Z_{rel} are dimensionless parameters of order unity describing the gas disk mass and metalicity respectively [Chiang and Youdin (2010)]. Because protoplanetary disk flows are thought to be highly turbulent, this thickness requirement is difficult to satisfy. However, incorporating the effects of gas drag on the dust can help relax equation (3). When drag on the dust is included but back-reaction on the gas is neglected, the dispersion relation for density perturbations from which Toomre's criterion is derived becomes

$$\omega = i(c^2k_r^2 - 2\pi G\Sigma|k_r|)t_s \tag{5}$$

where t_s is the time it takes for the gas to reduce a dust particle's velocity by order unity [Chiang and Youdin (2010)]. This new dispersion relation reveals that waves are unstable if $k_r < 2\pi G\Sigma/c^2$ even if $Q > 1$. Furthermore, numerical simulations reveal that graviational collapse of solids due to the gravitational instability occurs over timescales fast enough to overcome the one-meter hurdle and prevent the solid body from crashing into the central star [Johansen et al. (2007)].

However, while the gravitational instability model could offer a potential solution to the

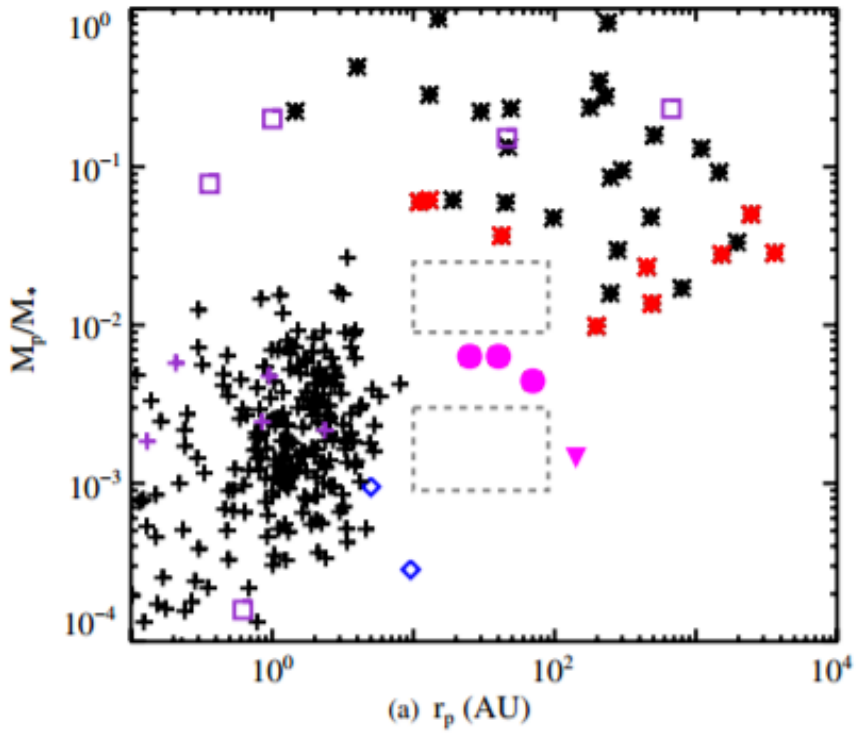

Figure 2: Figure from Kratter et al. (2010) showing the distribution of the masses of celestial bodies. The "brown dwarf desert" Matzner and Levin (2005) is highlighted with dashed boxes.

one-meter hurdle, it is not without problems of its own. GI essentially claims that the same fundamental physical processes govern the formation of both stars and planets. However, there is a noticeable lack of celestial bodies between the mass of the largest planets and the mass of the smallest stars [Zuckerman and Song (2009), see figure 2]. If planet and star formation both operated under the same processes, we would expect to observe a continuum of masses. Consequently, it seems likely that planet and star formation are fundamentally different processes, and more celestial bodies within this "brown-dwarf desert" [Matzner and Levin (2005)] need to be observed to provide robust physical evidence of the GI model

Another potential alternative to the core-accretion model is known as the streaming instability [Youdin and Goodman (2005)]. Because the gas in a protoplanetary disk exerts drag on dust particles, by Newton's Third Law, the dust must exert an equal and opposite force back on the gas. Youdin and Goodman (2005) incorporate this back-reaction when assessing the stability of perturbations within the disk. After assuming azimuthal symmetry and ignoring variations in z, they derive a sixth-order dispersion relation that generates instabilities as the particle density within the midplane approaches the gas density. These instabilities primarily serve to clump particles together, coagulating them into large fragments over time scales fast enough

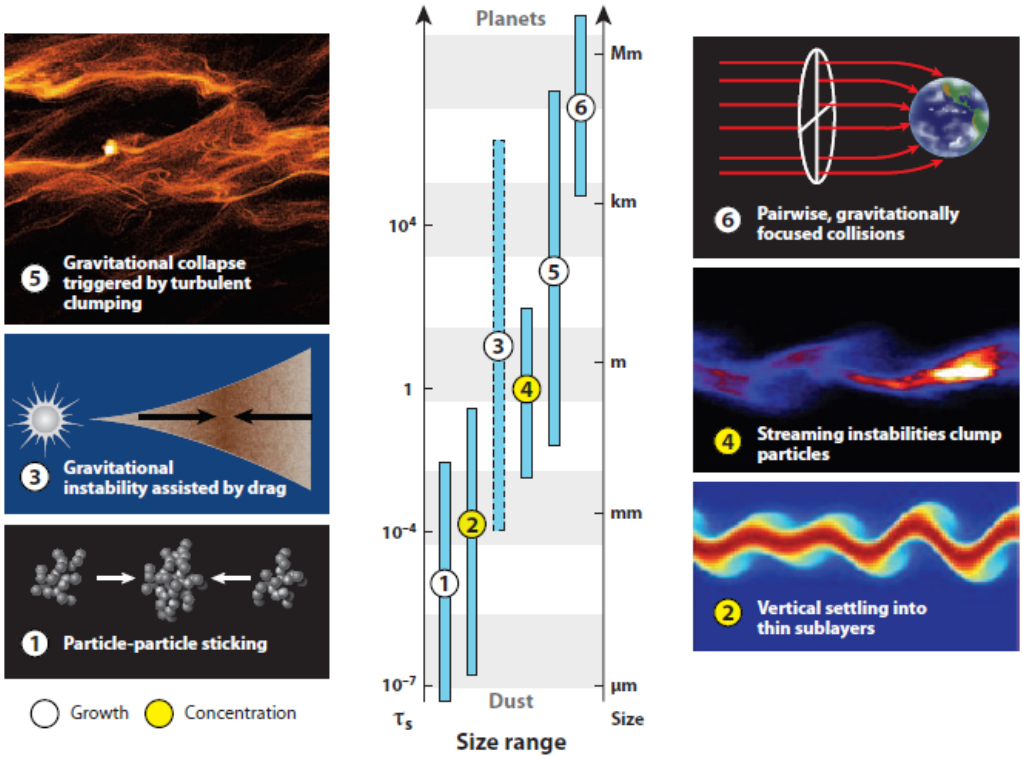

Figure 3: Summary of the processes that can build planets in a proto-planetary disk, as well as the length scales over which each process is relevant. Source: Chiang and Youdin (2010)

to overcome the one-meter hurdle [Youdin and Goodman (2005)]. Additionally, Youdin and Johansen (2007) verify the growth of these instabilities using numerical simulations, revealing the promise of a fluid-dynamics approach to planetesimal formation.

So far I have described the features and pitfalls of several theories on planetesimal formation. Each of these theories establishes a relatively complicated model of a protoplanetary disk and then explores how that model evolves over time. The purpose of this thesis is to apply the same technique to a much simpler model of the early solar system, namely, a single-phase, axisymmetric, rotating ideal, dusty-gas disk. We observe how perturbations to this simple model evolve in space and time, and then posit what those observations reveal about the processes that effect the evolution of the solar system, including planetesimal formation. I do not set out to develop a new model to replace core accretion, GI or the streaming instability or to solve the one-meter hurdle or planetary migration. Rather my goal is simply to explore what insight a simplified model can reveal about the processes described by these theories.

Simple Orbital Perturbations

Before exploring the equations of a gas disk, I briefly examine the behavior of a solid body rotating around a star though a vacuum. In this two-body model, I treat the star as a stationary point mass, and the only force acting on the body is the gravity from the star. In such a scenario, the equations for the conservation of linear and angular momentum can be written as

$$\frac{\partial v_r}{\partial t} + v_r \frac{\partial v_r}{\partial r} - \frac{v_\phi^2}{r} = -\frac{GM}{r^2} \tag{6}$$

$$\frac{\partial v_\phi}{\partial t} + \frac{v_r}{r}\frac{\partial}{\partial r}(r v_\phi) = 0 \tag{7}$$

where M is the stellar mass, G is the universal gravitational constant, and v_r v_ϕ are the radial and angular velocities of the body respectively. The radial and angular velocities of the planet can be written as the sum of a steady background velocity that varies only with radius and small perturbations that vary with both radius and time. Such representations take the form

$$v_r = w_0(r) + \epsilon w_1(r,t) \tag{8}$$

$$v_\phi = v_0(r) + \epsilon v_1(r,t) \tag{9}$$

where ϵ is small, w_0 and v_0 represent the background radial and angular velocities, and w_1 and v_1 represent the perturbations to the background states. Substituting these new definitions and collecting terms of the same order in ϵ, (6) and (7) become

$$w_0 \frac{\partial w_0}{\partial r} - \frac{v_\phi^2}{r} = -\frac{GM}{r^2} \tag{10}$$

$$\frac{\partial w_1}{\partial t} + w_0 \frac{\partial w_1}{\partial r} + w_1 \frac{\partial w_0}{\partial r} - \frac{2 v_0 v_1}{r} = 0 \tag{11}$$

$$w_0 \left(\frac{v_0}{r} + \frac{\partial v_0}{\partial r} \right) = 0 \tag{12}$$

$$\frac{\partial v_1}{\partial t} + \frac{w_0 v_1 + w_1 v_0}{r} + w_0 \frac{\partial v_1}{\partial r} + w_1 \frac{\partial v_0}{\partial r} = 0 \tag{13}$$

Since ϵ is small, I have neglected terms of order ϵ^2. If there is no background radial velocity $(w_0 = 0)$, then from (10), it follows that

$$v_\phi = \sqrt{\frac{GM}{r}} = v_k \tag{14}$$

Equation (14) is simply the definition of the Keplerian velocity. Thus, in the absence of of radial drift, a solid body at a distance r from the sun will, unsurprisingly, orbit the sun in a circle at the Keplerian velocity.

The dynamics of the body's orbit become more interesting when we consider the perturbations to this background state. Substituting (14) into (11) and (13) gives

$$\frac{\partial w_1}{\partial t} - 2v_1\sqrt{\frac{GM}{r^3}} = 0 \tag{15}$$

$$\frac{\partial v_1}{\partial t} + w_1\left(\frac{1}{2}\sqrt{\frac{GM}{r^3}}\right) = 0 \tag{16}$$

Furthermore, substituting (16) into $\frac{\partial}{\partial t}$(15)

$$\frac{\partial^2 w_1}{\partial t^2} = -\omega_k^2 w_1 \tag{17}$$

where $\omega_k \equiv \sqrt{\frac{GM}{r^3}}$ is the Keplerian orbital frequency. Substituting (15) into $\frac{\partial}{\partial t}$(16) produces an identical differential equation for v_1. The solution to these differential equations are

$$w_1 = A\sin(\omega_k t) + B\cos(\omega_k t) \tag{18}$$

$$v_1 = \frac{A\cos(\omega_k t) - B\sin(\omega_k t)}{2} \tag{19}$$

where A and B are determined by the initial conditions of the body's orbit. Equations (18) and (19) state that perturbations to the base radial and angular velocity oscillate around the base circular orbit at the Keplerian frequency. These equations also parametrize an elliptical orbit. Again, this is not a surprising result, as (18) and (19) show that linear perturbation of the two-body momentum equations is a method of deriving Kepler's first law.

So far, the results we have described rare neither surprising or novel. The purpose of this exercise was simply to understand how perturbations evolve in a simple model of our solar system to serve as a reference for our more complex model described in the following sections. I hypothesize that incorporating gas pressure into the model would result in similar oscillatory behavior.

Gas Disk Model: Governing Equations

I now examine how gas pressure effects velocity perturbations in an early solar system. To begin, I treat the early solar system simply as a disk of gas and dust orbiting around a star of mass M. The gas and dust are phase locked; both phases travel at the same velocity throughout the disk and exert no force on each other. The governing equations of such a "dusty gas" system are the continuity equation and the Navier-Stokes Equations

$$\frac{\partial \rho}{\partial t} + \nabla \cdot (\rho \vec{v}) = 0 \tag{20}$$

$$\frac{D\vec{v}}{Dt} = -\frac{\nabla p}{\rho} + \nu \nabla^2 \vec{v} + \vec{F_b} \tag{21}$$

where $\vec{v}$ is the velocity of the dusty gas, ρ is the fluid density, p is the pressure, ν is the kinematic viscosity, and $\vec{F_b}$ are the body forces acting on the fluid. In this system, the primary body force is gravity, which is given as

$$\vec{F_b} = \nabla \left(\frac{GM}{r} \right) \tag{22}$$

Equations (20) and (21) describe the behavior of any fluid; however, for our system, we can make some assumptions about the structure of the disk to make these equations easier to work with.

1. **The gas disk is inviscid**, allowing us to eliminate all terms containing ν.

2. **The disk has azimuthal symmetry.** When working in cylindrical polar coordinates (r, ϕ, z), this assumption enables us to set all $\frac{\partial}{\partial \phi}$ terms eqal to 0. Like in Youdin and Goodman (2005), I still consider the dusty gas's angular velocity, but I assume that it does not vary in ϕ.

3. **The disk has a flared structure.** Understanding how the height of the disk varies with radius is necessary to determine how heat is transfered throughout the disk. Assuming a flared structure allows one to express the temperature T of the disk as a power function in r [Armitage (2010)]. i.e.

   $$T = T_0 \left(\frac{r}{r_0} \right)^{-n} \tag{23}$$

   where n is a postive number.

4. **We restrict our region of interest to the disk midplane.** Gravity eventually causes

most material within the disk to settle at the midplane, [Lin (2008)], and it is the region of the disk where planet formation is most likely. This assumption converts our system into a two-dimensional problem, allowing us to ignore varitations in the z-direction and dramatically simplifying the gravity term in equation (21).

5. **The equation of state of our fluid is that of an ideal gas.** In other words

$$p = \rho RT = c_s^2 \rho \tag{24}$$

where c_s is the gas sound speed and R is the specific gas constant.

These assumptions allow us to write (20) and (21) is cylindrical co-ordinates as

$$\frac{\partial \rho}{\partial t} + \frac{1}{r}\frac{\partial}{\partial r}(r\rho v_r) = 0 \tag{25}$$

$$\frac{\partial v_r}{\partial t} + v_r\frac{\partial v_r}{\partial r} - \frac{v_\phi^2}{r} = -\frac{1}{\rho}\frac{\partial p}{\partial r} - \frac{GM}{r^2} \tag{26}$$

$$\frac{\partial v_\phi}{\partial t} + \frac{v_r}{r}\frac{\partial}{\partial r}(rv_\phi) = 0 \tag{27}$$

where v_r and v_ϕ are the angular and radial velocities respectively. Using (23) and (24) to express pressure in terms of ρ and T, (26) becomes

$$\frac{\partial v_r}{\partial t} + v_r\frac{\partial v_r}{\partial r} - \frac{v_\phi^2}{r} = -\frac{R}{\rho}\left(T\frac{\partial \rho}{\partial r} + \rho\frac{\partial T}{\partial r}\right) - \frac{GM}{r^2} \tag{28}$$

$$\frac{\partial v_r}{\partial t} + v_r\frac{\partial v_r}{\partial r} - \frac{v_\phi^2}{r} = -\frac{c_s^2(r)}{\rho}\left(\frac{\partial \rho}{\partial r} - \frac{n\rho}{r}\right) - \frac{GM}{r^2} \tag{29}$$

where $c_s^2(r) \equiv RT_0\left(\frac{r}{r_0}\right)^{-n}$. Thus, equations (25), (27), and (29) fully describe the evolution of gas density and velocity within the disk.

Before we examine how the gas properties evolve over time, one must first define a steady-state solution in which the disk properties remain constant in time $\left(\frac{\partial}{\partial t} = 0\right)$. Such a state can be achieved by also specifying that $v_r = 0$. In this state (25) and (27) become trivial, but (29) reveals that pressure and gravity cause the gas to orbit at the sub-Keplerian orbital velocity

$$v_\phi = \sqrt{v_k^2 + \frac{c_s^2}{\rho}\left(\frac{\partial \rho}{\partial r} - \frac{n\rho}{r}\right)} \tag{30}$$

Table 1: **Non-dimensional Parameters**

Symbol	Meaning	Value Range	Equation Number
α	Dimensionless Keplerian Velocity	$10 - 10^3$	(39)
n	Temperature Profile Exponent	$3/7 - 1$	(23)
m	Density Profile Exponent	$1/2 - 2$	(44)

Table 2: **Non-dimensional Variables**

Variable	Meaning	Equation
f	Non-dimensionalized density	(44)
w	Non-dimensionalized radial velocity	(42)
u	Non-dimensionalized angular velocity	(43)
η	Normalized density perturbation	
ψ	Normalized angular velocity perturbation	
$\hat{r}$	Non-dimensionalized radial distance	(31)
$\hat{t}$	Non-dimensionalized time	(31) (32)

Thus the background steady for this model is the scenario described by equation (1), in which the dusty gas orbits the central star in a circle at a sub-Keplerian velocity.

Non Dimensionalization and Perturbation

Now that a steady state has been defined, one can use dimensional analysis to understand the relative importance of each term in each equation. This system has three key variables: distance, velocity, and density, and we redefine these variables as follows:

$$r = L\hat{r} \tag{31}$$

$$v = V\hat{v} \tag{32}$$

$$\rho = \Phi\hat{\rho} \tag{33}$$

where L, V, and Φ are the characteristic length, velocity, and density scales and the hatted variables are now dimensionless. With these new definitions, the governing equations become

$$\frac{\Phi V}{L}\left(\frac{\partial\hat{\rho}}{\partial\hat{t}} + \frac{1}{\hat{r}}\frac{\partial}{\partial\hat{r}}(\hat{r}\hat{\rho}\hat{v_r})\right) = 0 \tag{34}$$

$$\frac{V^2}{L}\left(\frac{\partial\hat{v_\phi}}{\partial\hat{t}} + \frac{\hat{v_r}}{\hat{r}}\frac{\partial}{\partial\hat{r}}(\hat{r}\hat{v_\phi})\right) = 0 \tag{35}$$

$$\frac{\partial \hat{v_r}}{\partial \hat{t}} + \hat{v_r}\frac{\partial \hat{v_r}}{\partial \hat{r}} - \frac{\hat{v_\phi}^2}{\hat{r}} = -\frac{RT}{V^2 L^n}\left(\frac{\hat{r}}{r_0}\right)^{-n}\left(\frac{\partial \hat{\rho}}{\partial \hat{r}} - \frac{n\hat{\rho}}{\hat{r}}\right) - \frac{GM}{V^2 L}\frac{1}{\hat{r}^2} \tag{36}$$

We can ensure that all hatted variables are of order 1 by defining L and V such that

$$L \equiv r_0 \tag{37}$$

$$V \equiv \sqrt{RT_0} = c_{s0} \tag{38}$$

Substituting these definitions into (25), (27), and (29) and removing the hats gives the non-dimensionalized equations of continuity, angular momentum, and radial momentum respectively. The non-dimensionalized continuity and angular momentum equations will look identical to (25) and (27), but the non-dimensionalized radial momentum equation is

$$\frac{\partial v_r}{\partial t} + v_r\frac{\partial v_r}{\partial r} - \frac{v_\phi^2}{r} = -r^{-n}\left(\frac{\partial \rho}{\partial r} - \frac{n\rho}{r}\right) - \frac{\alpha^2}{r^2} \tag{39}$$

The new parameter, α, is defined such that

$$\alpha^2 \equiv \frac{GM}{c_{s0}^2 r_0} \tag{40}$$

In other words,α specifies the ratio of the of the Keplerian velocity to the gas sound speed at $r = r_0$. Because the rest of the terms in (39) are of order 1, the magnitude of α^2 determines the behavior for the radial momentum equation. The value of α^2 can vary from solar system to solar system as it depends heavily on the temperature and mass of the central star, but for the purposes of this analysis, I consider values of α^2 between 10^2 and 10^4

After non-dimensionalizing, the next step is to linearize the governing equations about the steady-state described in the previous section. This is done by redefining our variables ρ, v_r, and v_ϕ as the sum of the background steady and small perturbation that vary with time:

$$\rho(r,t) = f_0(r) + \epsilon f_1(r,t) \tag{41}$$

$$v_r(r,t) = \epsilon w_1(r,t) \tag{42}$$

$$v_\phi(r,t) = u_0(r) + \epsilon u_1(r,t) \tag{43}$$

where $f_1, w_1, u_1 \ll f_0, u_0$. Furthermore, it is assumed that the unperturbed density f_0 behaves

as a power function with respect to r, i.e.

$$f_0 \propto r^{-m} \tag{44}$$

where m is a positive number. Algebraic manipulation transforms the non-dimensionalized governing equations (25), (27) and (39) into

$$\frac{\partial \eta}{\partial t} + \frac{\partial w_1}{\partial r} + \frac{w_1}{r}(1-m) = 0 \tag{45}$$

$$v = r^{-n}\left(\frac{r}{f_0}\frac{\partial f_0}{\partial r} - n\right) + \frac{\alpha^2}{r} = -r^{-n}(m+n) + \frac{\alpha^2}{r} \tag{46}$$

$$\frac{\partial w_1}{\partial t} - \frac{2v^2\psi}{r} - \frac{v}{r}\eta = -r^{-n}\left(\frac{\partial \eta}{\partial r} - \frac{(m+n)\eta}{r}\right) - \frac{\alpha^2}{r^2}\eta \tag{47}$$

$$\frac{\partial \psi}{\partial t} + \frac{w_1}{2v}\frac{\partial v}{\partial r} + \frac{w_1}{r} = 0 \tag{48}$$

where $\eta \equiv \frac{f_1}{f_0}$, $\psi \equiv \frac{u_1}{u_0}$, and $v \equiv u_0^2$.

The final step of this linear perturbation analysis is to combine all four of these equations into a single expression that describes how the perturbations evolve over time. Substituing $\frac{\partial}{\partial r}$ of (45), (46), and (48) into $\frac{\partial}{\partial t}$ of (47) gives

$$r^n\left(\frac{\partial^2 w_1}{\partial t^2} + \frac{w_1}{r}\left(\frac{\alpha^2}{r^2} + \frac{n(m+n) - 2(m+n)}{r^{n+1}}\right)\right) = (1-m)\frac{\partial}{\partial r}\left(\frac{w_1}{r}\right) + \frac{\partial^2 w_1}{\partial r^2} \tag{49}$$

(49) is a partial differential equation of w_1 alone. If we assume that the time dependence of w_1 goes as $e^{i\omega t}$, then we can solve this equation numerically using MATLAB's boundary-value-problem-solving tool.

The following figures show plots of the numerical solutions to this equation for different values of n, m, α^2. I achieve this solution by starting with a mesh of 10,000 points spanning from $r = 0$ to $r = 30$. The characteristic length scale corresponds to a length of 1AU, and $r = 30$ represents the outer limit of the disk. ω is set to 1 in all figures to make changes to the oscillatory behavior easily observable. Perturbations are driven at the outer edge of the solar system and die off once they reach the central star. These criteria are represented in the model through the boundary conditions $w_1(r = 0.01) = 0$ and $w_1(r = 30) = 1$ (setting $w_1(r = 0) = 0$ results in a singularity). The amplitude of perturbations is set to one because, to quote Youdin and Goodman (2005), "perturbation amplitudes are arbitrary in a linear analysis."

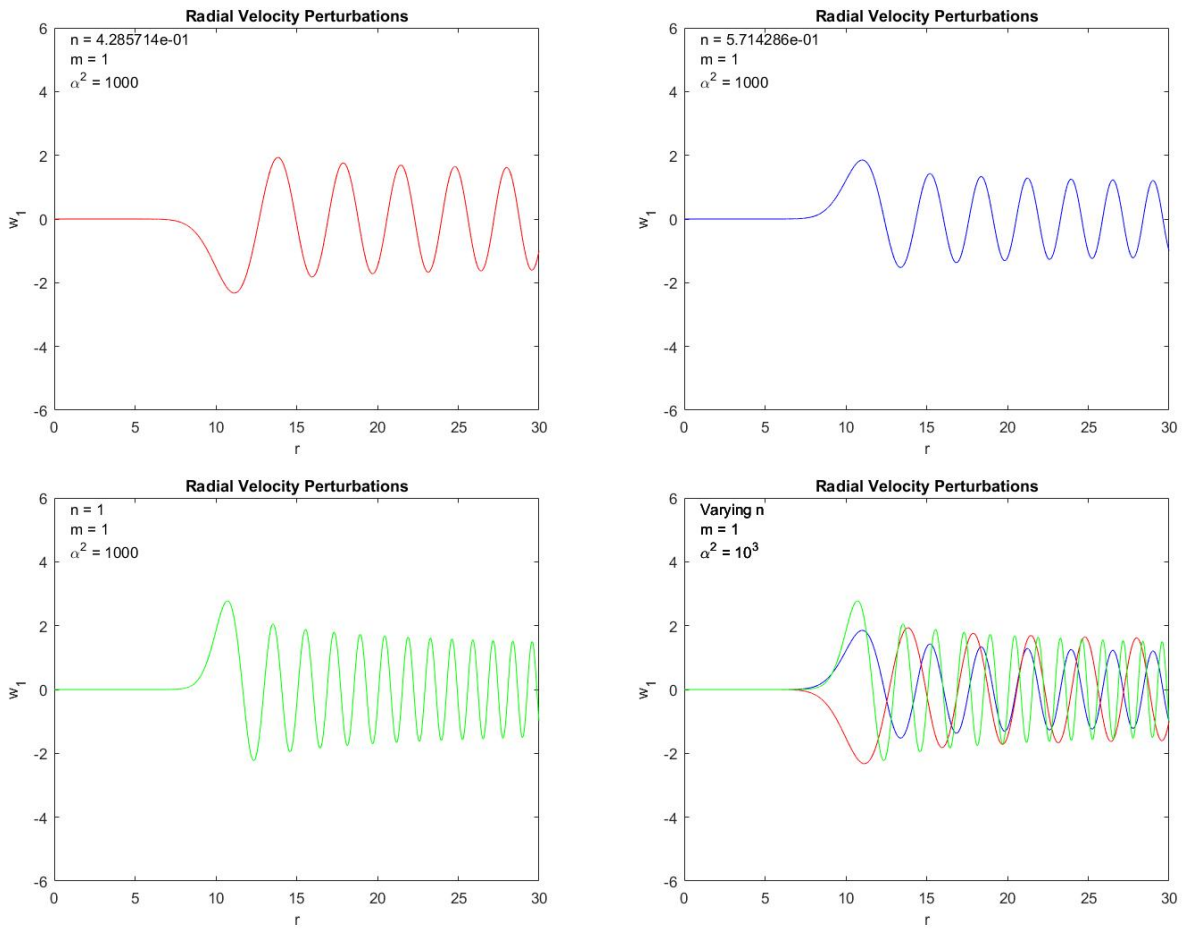

Figure 4: Plots showing the numerical solutions to equation (49) for $m = 1$, $\alpha^2 = 10^3$, and varying values of n. *Top Left:* $n = 3/7$ *Top Right:* n = 4/7 *Bottom Left:* n = 1 *Bottom Right:* All three plotted together. Increasing n increases both the wave number of the solution and the amplitude of the initial oscillation. Variations in n have no effect on the radius of initial oscillation r_{osc}.

Only inward-propagating solutions to this differential equation because beyond $r = 30$, it is assumed that $\rho = 0$ and there is no more material through which the wave can propagate.

From these numerical solutions, it is clear that perturbations to the radial velocity are zero at within the inner portions of the disk, before beginning to oscillate at some radius r_{osc}. Since the only boundary an inward-propagating wave will encounter is at the center of the disk, this phenomenon justifies the exclusion of the effects of reflected waves in the analysis. Figure 4 shows that varying n (the power of the temperature profile)does not change the overall structure of the perturbation function or r_{osc}. A change in n simply changes the wave number of the oscillations, with larger n corresponding to larger wave numbers. Similarly, figure 5 shows that varying m (the power of the density profile) only alters the amplitude of the initial

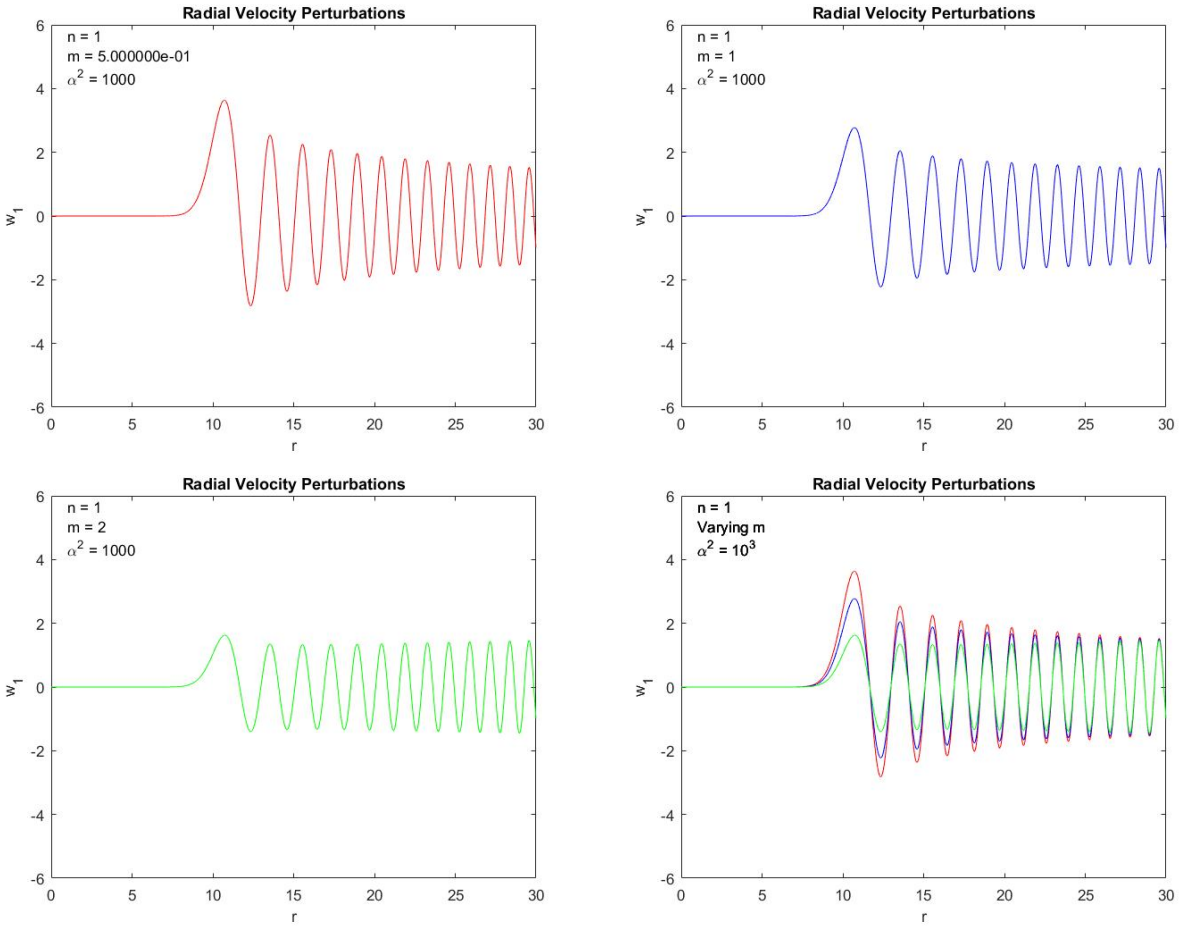

Figure 5: Plots showing the numerical solutions to equation (49) for $n = 1$, $\alpha^2 = 10^3$, and varying values of m. *Top Left:* $m = 1/2$ *Top Right:* m = 1 *Bottom Left:* m = 2 *Bottom Right:* All three plotted together. Increasing m increases only the amplitude of the innermost oscillation. The wave number and r_{osc} are both unaffected by changes in m.

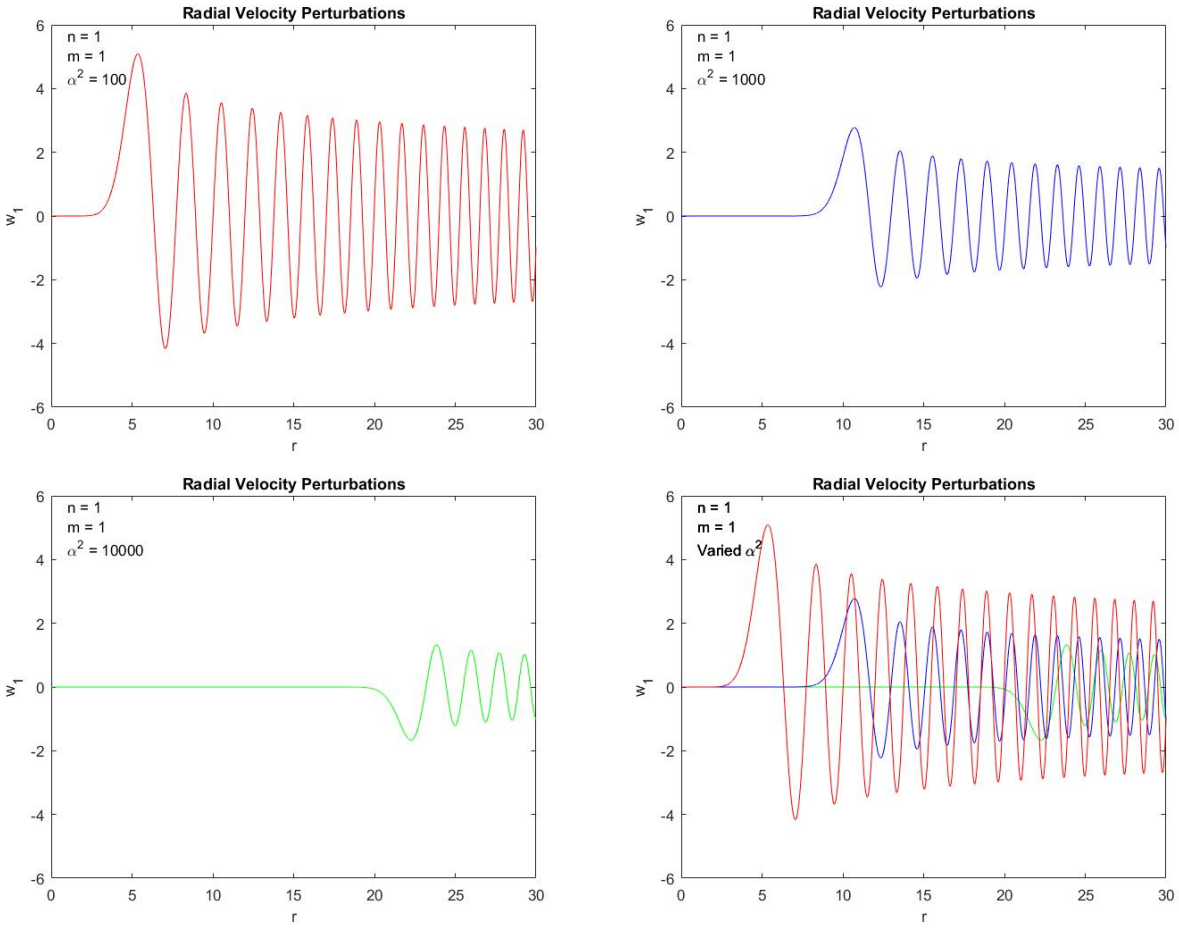

Figure 6: Plots showing the numerical solutions to equation (49) for $n = 1$, $m = 1$, and varying values of α^2. *Top Left:* $\alpha^2 = 10^2$ *Top Right:* $\alpha^2 = 10^3$ *Bottom Left:* $\alpha^2 = 10^4$ *Bottom Right:* All three plotted together. Changes in α^2 affect all three key components of the solution's structure. Increasing α^2 decreases the wave number and the amplitude, but increases r_{osc}.

osciallation; both the wave number and r_{osc} are resistant to changes in m. However, figure 6 reveals that varying α^2 results in more interesting and dramatic changes. An increase in α^2 not only decreases the amplitude of the innermost perturbation, it also decreases the wave number and increases r_osc. Thus, the ratio between the Keplerian velocity and the gas sound speed is the most important parameter for determining the structure of radial velocity perturbations within a single-phase protoplanetary disk.

The numerical solutions in figures 4, 5, and 6 have yielded lots of useful information about the effects of the free parameters on radial velocity perturbations. To gain additional insight, I now search for a specific scenario for which I can derive an analytical solution for w_1. As it happens, $n = 1$ is just such a scenario. The results of this analysis are presented in the following section.

Searching for an Analytic Solution

As discussed above, varying n in (49) only chnages the wave number of the solutionn to w_1, not the overall behavior or radius of initial oscillation. Thus, we can learn more about the behavior of w_1 by searching for analytic solutions valid for particular n. If we assume that $n = 1$ and that the t-dependence of w_1 behaves as $e^{i\omega t}$, then (49) becomes

$$r^2 w'' + r(1-m)w' + (r^3\omega^2 - \beta^2)w = 0 \tag{50}$$

where $\beta^2 \equiv \alpha^2 - 2m$, $w' \equiv \frac{\partial w_1}{\partial r}$, and $w'' \equiv \frac{\partial^2 w_1}{\partial r^2}$. This is a second order differential equation with a form similar to that of the Bessel function, and with a few minor changes of coordinates, (50) can be rewritten in the form of the Bessel function differential equation. Defining $u \equiv r^\gamma$, (50) becomes

$$\gamma^2 u^2 w'' + (\gamma - m)\gamma u w' + (u^{3/\gamma}\omega^2 - \beta^2)w = 0 \tag{51}$$

where w' and w'' now refer to $\frac{\partial w_1}{\partial u}$ and $\frac{\partial^2 w_1}{\partial u^2}$ respectively. In attempting to get something that looks like a Bessel function are free to set our transformation parameter γ to whatever value we choose. For $\gamma = 3/2$, (51) becomes

$$\gamma^2 u^2 w'' + (\gamma - m)\gamma u w' + (u^2\omega^2 - \beta^2)w = 0 \tag{52}$$

making the additional transformation $w = u^a f(u)$, (52) becomes

$$u^2 f'' + uf' + \left(u^2 \left(\frac{\omega}{\gamma} \right)^2 - \delta^2 \right) f = 0 \tag{53}$$

where $\delta^2 \equiv \frac{\beta^2}{\gamma^2} - \frac{m}{\gamma}$. The solution to (53) is a Bessel function in u. Therefore, the final solution to w_1 is

$$w_1 = r^{m/2} \left(C_1 J_\delta \left(r^{3/2} \frac{2\omega}{3} \right) + C_2 Y_\delta \left(r^{3/2} \frac{2\omega}{3} \right) \right) e^{i\omega t} \tag{54}$$

where C_1 and C_2 are specified by the boundary conditions. Imposing the boundary conditions from the previous section gives

$$C_1 = \frac{Y_\delta(0)}{30^{m/2} * \left(J_\delta \left(30^{3/2} \frac{2\omega}{3} \right) * Y_\delta(0) - J_\delta(0) * Y_\delta \left(30^{3/2} \frac{2\omega}{3} \right) \right)} \tag{55}$$

$$C_2 = -\frac{J_\delta(0)}{30^{m/2} * \left(J_\delta \left(30^{3/2} \frac{2\omega}{3} \right) * Y_\delta(0) - J_\delta(0) * Y_\delta \left(30^{3/2} \frac{2\omega}{3} \right) \right)} \tag{56}$$

Figure 7 compares MATLAB plots of (54) and (49) when $n = 1$, $m = 1$, and $\alpha^2 = 1000$. A plot showing the difference between the numerical and analytical solutions ((49) - (54)) has also been included. These plots reveal that there is a roughly 3% error between the two solutions. I believe that that this error is a result of the highly oscillatory behavior of the solution, which makes it difficult for MATLAB to find a numeric solution within our specified residual of 0.01. This agreement between the numerical and analytical solutions to the problem allows us to use the Bessel function described by equation (54) as a basis for developing a deeper understanding of how these waves propagate through the model protoplanetary disk.

Discussion

The major motivation underlying this research was to gain insight into the dynamics at play within the solar system during its earliest stages and to see whether these insights could help solve unanswered questions regarding the evolution of bodies in the early solar system. This single-phase model can be thought of as a simplification of GI [Boss (1997)] and streaming instability [Youdin and Goodman (2005)] models, which attempt to overcome the one meter-hurdle. This model shows that even in a simple, single-phase gas disk, radial velocity perturbations create regions of convergence $\frac{\partial w_1}{\partial r} > 0$ and regions of divergence $\frac{\partial w_1}{\partial r} < 0$. Because of

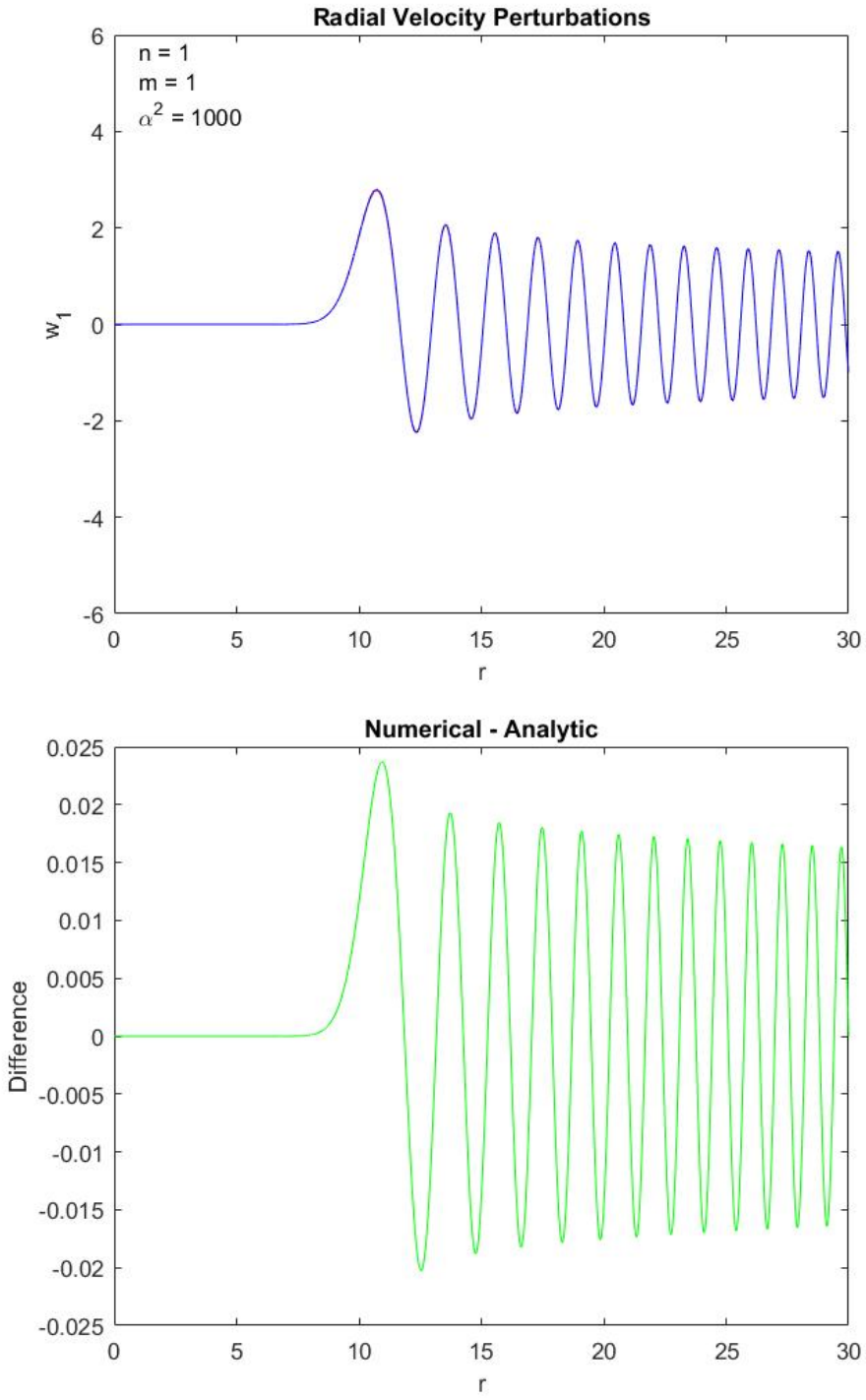

Figure 7: *Left:* MATLAB plot of the numerical (red) and analytical solutions (blue) to (49) for $n = 1$, $m = 1$, and $\alpha^2 = 10^4$. *Right:* Difference between numerical and analytical solutions. The 3% discrepency between the solutions is likely the result of the oscillatory behavior, and the difficulty associated with getting a numerical solution with a small residual.

this phenomenon, gas will tend to accumulate in regions of the disk where $w_1 = 0$ and $\frac{\partial w_1}{\partial r} < 0$. Thus, a driven perturbation at the outer edge of a protoplanetary disk can still cause material to accumulate several AU inward of the perturbation. These regions of accumulation, like the snow line [Lin (2008)], are prime locations for planetesimal formation. Therefore, perturbations at the outer edge of the planetary disk can generate density maxima at smaller radii that can spawn young planets.

Alternatively, one can consider these velocity perturbations as sound waves propagating energy from the out solar system to the inner solar system. If the perturbation were being driven by an orbiting planet, this sound wave could be a mechanism of removing energy from the planet's orbit. This energy loss would cause the planet to slow down and lose angular momentum, which in turn would cause it to sprial inward. These sound waves would continue to remove energy from the planet's orbit until eventually the planet reached a radius (determined by δ) at which the wave dies out. This removal of energy through sound waves could be a potential mechanism drivng planetary migration. It explains how planets that originally form at the outer regions of the solar system can travel inward, and it also explains why the migration stops at a particular radius, preventing the planet from crashing into the central star.

In generalizing these solutions to real protoplanetary disks, it becomes important to reevaluate the initial assumptions and decide if there are regions within the disk or times within the disk's life cycle where these assumptions may break down. Since the composition of protoplanetary disks is a complex mixture of light gases and metals, the smooth density profile described by equation (44) is perhaps the weakest assumption. As described in in Lin (2008), in a real protoplanetary disk, volatiles such as water will transition from the gas to solid phase at radii corresponding to their boiling points, causing the composition of the gas to change as one moves farther away from the central star. Similarly, if the relevant density profile changes with radius, then the relevant α^2 parameter may vary with radius as well. One possible way to address this behavior would be to impose a piece-wise density profile of several varying power laws, with function breaks occurring at radii corresponding to the boiling points of key volatiles. One could then combine these functions by requiring continuity of pressure and temperature at each break point, thereby creating a more realistic model of a protoplanetary disk.

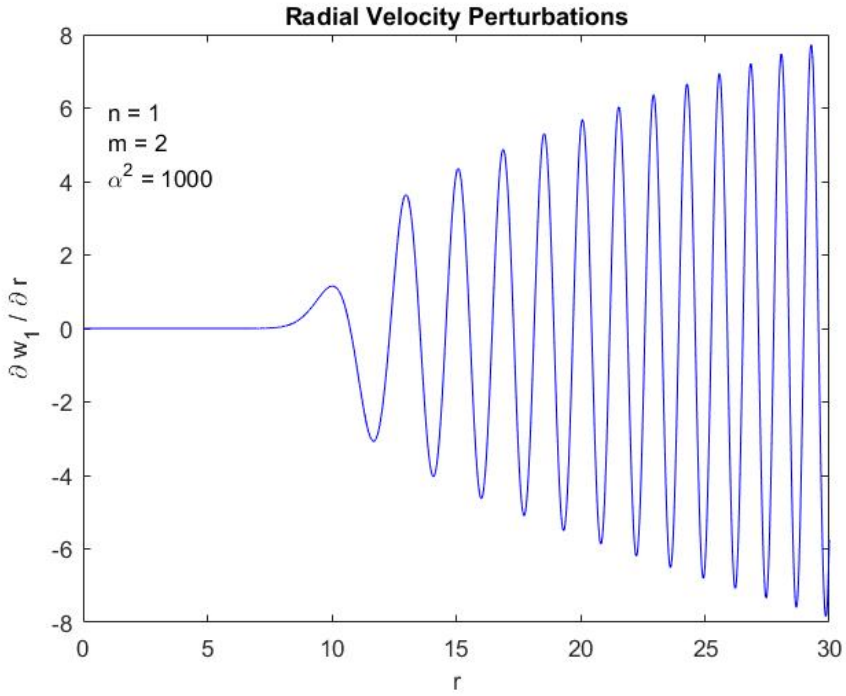

Figure 8: The derivative of w_1 for $n = 1$, $m = 1$, and $\alpha^2 = 10^3$. Matter is expected to accumulate in regions where $\frac{\partial w_1}{\partial r} < 0$, which could potentially lead to increased rates of planetesimal formation.

Future Directions

There are many potential avenues for future research to be conducted from this simple model of a protoplanetary disk. This thesis presents a simple, foundational model of the early solar system, and there are several additional forces and more complicated geometries at play. For example, in this model, I have assumed that perturbations to the radial velocity are axisymmetric, i.e. that they take the form of an annulus encircling the central star. True perturbations are likely not axisymmetric; however, the effects of non-axisymmetric perturbations on gravitational instabilities is still an open field of study. Noh et al. (1991) explore the non-axisymmetric linearly perturbed mass and momentum equations, and find several unstable growth modes for sufficiently massive disks. Tanga et al. (2004) test these predictions through N-body simulations of planetesimal clusters, but find that these perturbations evolve into instabilities only when gas drag is introduced. Furthermore, the drag levels they introduce, by their own admission, do not necessarily correspond to the levels of gas drag observed in physical protoplanetary disks. Non-axisymmetric perturbations have been shown to create vorticies in a disk that could form a planetary embryo, but only in the later stages of the disk's lifecycle, after a gas giant has already formed [de Val-Borro et al. (2007)].

The vertical structure of a protoplanetary disk must also be considered when analyzing the stability of perturbations. As mentioned earlier, Toomre's criterion (equation(4)) requires that the dust midplane layer reach a minimum thickness in order for gravitational instabilities to develop. However, vertical shear between different layers within the disk can prevent this criteria from being met by creating Kelvin-Helmholtz instabilities (KHI). However, raising the metallicity of the midplane (the Z_{rel} parameter in equation (4)), could potentially overcome this problem. Metallicity can be enriched through a variety of mechanisms, most notably through photoevaporation of the gas [Armitage (2011)] and through radial pile-up [Youdin (2003)]. Youdin and Shu (2002) show that, depending on the disk parameters, gravitational instabilities can manifest in midplanes with Z_{rel} values as low as two, thereby overcoming the issues introduced by vertical shear.

In addition to incorporating these additional components of the disk's geometry, any comprehensive model of protoplanetary disk evolution must be able to explain the transport of angular momentum throughout the disk. In my model, I neglected the background radial velocity drift in order to find the steady state solution to the governing equations. However, real protoplanetary disks exhibit no such stable behavior. In the early stages of the disk's life time, matter is accreting onto the central star, fueling it's growth. As such, angular momentum must be transported outward, away from the star, in order to achieve this mass flux [Armitage (2011)]. There are several mechanisms through which this transport can take place, but the most important, according to Armitage (2011) are self-gravity-induced gravitational instabilities (see **Alternate Hypotheses**) and the magneto-rotational instability (MRI). The magneteo-rotational instability posits that in the presence of a weak magnetic field, the orbits of rotating charged particles will be unstable if $\frac{d}{dr}(\Omega^2) < 0$. This criterion is always satisfied in a protoplanetary disk; however, the relevant importance of this instability compared the other forces within the disk is still an active area of investigation [Armitage (2011)].

The ultimate goal of models such as those in Youdin and Goodman (2005) that employ the methods described above is to develop a comprehensive, two-phase model of a protoplanetary disk and how all the relevant forces within the disk affect instabilities. Youdin and Goodman (2005) make an important start by incorporating both gas drag and dust back-reaction into their model, but a complete model of such as system would incorporate additional forms of phase interaction such as turbulence into the governing equations. Such an approach has shown to yield valuable insight in other geophysical systems. Bercovici and Michaut (2010) developed

such as model to explain the discrepancies between observed sound speeds in volcanoes and those predicted by the pseudo-gas theory. By including terms that quantified the phase interactions and fluid surface tension within a volcano, they were able to recreate the observed sound speeds from the relevant continuity, momentum, and energy equations. A similarly complete approach for a model protoplanetary disk will hopefully reconcile the discrepancies between theoretical limits on particle growth and observations from distant solar systems.

Summary and Conclusions

In this essay, I have shown that in a single-phase gas disk orbiting a point mass star, with temperature and density as power functions in r, perturbations in radial velocity will exhibit oscillatory behavior for real values of ω. When $T \propto r^{-1}$, and $p \propto r^{-}m$, the radial perturbations take the form of a transformed Bessel function of order δ multiplied by $r^{m/2}$. We find that most important parameter that determines the structure of the oscillations is α, the ratio between the Keplerian velocity and gas sound speed. I theorize that driven velocity perturbations at the outer edge of the solar system could offer plausible mechanisms for both overcoming the one-meter hurdle and halting planetary migration. Further investigations in this area should incorporate more complicated disk geometries and additional forces, with the ultimate goal to develop a two-phase gas and dust model.

Acknowledgments

I would like to thank Dave Bercovici and Yoshi Miyazaki for their support, knowledge, and guidance throughout the course of this project. I would also like to thank the faculty of Yale's Geology and Geophysics department for their helpful questions and criticisms during the presentation leading up to this thesis, as well as the Geology and Geophysics department itself, for providing funding to begin this research during the summer of 2016.

Appendix: MATLAB Code for the Numerical Solution

The following MATLAB code ws used to generate the plots in Figure 7. Modifications to this code were used to generate all other plots in the paper.

```
function samp2
%Initial variables and parameters
r0 = 0.001;
r1 = 30;
rend = 50;
pts = 10000;
rbes = linspace(r0,r1,pts);
n = 1;
m = 1;
gamma = 3/2;
a = m/(2*gamma);

%Setting order and wavelength of bessel function
alphasq = 10^3;
bsq = alphasq - 2*m;
dsq = alphasq/gamma^2 - (gamma - m)*a/gamma - a*(a+1);
b = bsq^(1/2);
d = dsq^(1/2);
wsq = 1;
omega = wsq^(1/2);
omega2 = omega/gamma;
u = rbes.^gamma;
%Boundary Conditions for analytic Solution
j0 = besselj(d, omega2*r0^gamma);
j1 = besselj(d, omega2*r1^gamma);
y0 = bessely(d, omega2*r0^gamma);
y1 = bessely(d, omega2*r1^gamma);

```

```
29 c1 = y0/(r1^(gamma*a)*(j0*y1 - j1*y0));
30 c2 = j0/(r1^(gamma*a)*(j1*y0 - j0*y1));
31
32 fbes = c1*besselj(d, u.*omega2) + c2*bessely(d, u.*omega2);
33
34 %  which in this case is  0<z<1f
35 % call init1 on a 10-point grid for initial guess, and to set
      the grid
36 init1 = @(r) myinit(r, r0, r1);
37 solinit = bvpinit(linspace(r0,r1,pts),init1);
38
39 % call bvp4c to get the solution to the ODE specified in ode1
      and given
40 %  the boundary conditions specified in bc1, with this initial
       guess and grid
41 ode1 = @(r,f) mydiff(r,f,m,n,alphasq,wsq);
42 options = bvpset('RelTol', 1e-2);
43 sol = bvp4c(ode1,@bc1,solinit,options);
44
45 % get the grid
46 r=sol.x;
47 % get the solution
48 f=sol.y;
49
50 descr = 'n = %d\nm = %d\n\\alpha^2 = %g';
51 str1 = sprintf(descr, n, m, alphasq);
52 % plot it against the analytic solution to check
53 figure(1)
54 plot(r,f(1,:),'r-')
55 plot(rbes,u.^(a).*(fbes),'b-')
56 title('Radial Velocity Perturbations')
57 text(1,5,str1)
```

```
%,r,f(2,:),'b-')
xlabel('r')
ylabel('w_{1}')
axis([0 r1 -6 6])
hold on

%figure 2 plots the difference
figure(2)
plot(rbes,u.^(a).*(fbes) - f(1,:),'g')
title('Numerical - Analytic')
xlabel('r')
ylabel('Difference')

%v = 1/z - asq/(z^n)*(m+n);
%dv = -z^(-2)+n*asq*z^(-n-1)*(m+n);

%cs = (r^(-n));
%v = (asq/r - r^(-n)*(m+n));
%dvdr = (-asq*r^(-2) + n*r^(-n-1)*(m+n));
%-------------------------------------
function dfdz = mydiff(r,f,m,n,asq,wsq)
%   The 2nd order ODE  "d^2f/dz^2 =  -(pi/2)^2 f",
%   which becomes two 1st order ODEsi
%     df1/dz = f2     and    df2/dz  = -(pi/2)^2 f1
dfdz = [f(2)
        (r.^n).*(-wsq*f(1) + (f(1)./r).*(asq/r.^2 + (n-2)*(m+n
           )./r.^(n+1))) + (m-1)*(r.^(-1).*f(2) - f(1)./r.^2)];
end
%-------------------------------------


function res = bc1(fa,fb)
```

```
89 % Boundary condition that f(z=0) = 0, and f(z=1) = 1
90 %  where fa is f at z=0,  fb at z=1.
91 res = [ fa(1)
92           fb(1) + 1];
93 end
94
95 %--------------------------------------
96
97 function v = myinit(r, r0, r1)
98     %f1 = -(z-z0)/(z1-z0);
99     %f2 = -1/(z1-z0);
100     f1 = -(r-r0)^2/((r1-r0)^2);
101     f2 = -2*(r-r0)/((r1-r0)^2);
102 % initial guess has to have the right boundary conditions
103 v = [ f1
104           f2];
105 end
106
107 end
```

Bibliography

Armitage, P. J. (2010). *Astrophysics of Planet Formation*. Cambridge UP, Cambridge UK.

Armitage, P. J. (2011). Dynamics of protoplanetary disks. *Annual Review of Astronomy and Astrophysics*, 49:195–236.

Bercovici, D. and Michaut, C. (2010). Two-phase dynamics of volcanic eruptions: Compaction, compression, and the conditions for choking. *Geophys. J. Int.*, 182:843–864.

Binney, J. and Tremaine, S. (2011). *Galactic dynamics*. Princeton university press.

Blum, J. and Wurm, G. (2008). The growth mechanisms of macroscopic bodies in protoplanetary disks. *Annual Review of Astronomy and Astrophysics*, 46:21–56.

Boss, A. P. (1997). Giant planet formation by gravitational instability. *Science*, 276:1836–1839.

Chiang, E. and Youdin, A. (2010). Forming planetesimals in solar and extrasolar nebulae. *Annual Review of Earth and Planetary Sciences*, 38:493–522.

Chokshi, A., Tielens, A., and Hollenbach, D. (1993). Dust coagulation. *The Astrophysical Journal*, 407:806–819.

de Val-Borro, M., Artymowicz, P., D'Angelo, G., and Peplinski, A. (2007). Vortex generation in protoplanetary disks with an embedded giant planet. *Astronomy & Astrophysics*, 471(3):1043–1055.

Doyle, L. R., Carter, J. A., Fabrycky, D. C., Slawson, R. W., Howell, S. B., Winn, J. N., Orosz, J. A., Prsa, A., Welsh, W. F., Quinn, S. N., et al. (2011). Kepler-16: a transiting circumbinary planet. *Science*, 333(6049):1602–1606.

Goodman, J. and Pindor, B. (2000). Secular instability and planetesimal formation in the dust layer. *Icarus*, 148(2):537–549.

Hayashi, C., Nakazawa, K., and Nakagawa, Y. (1985). Formation of the solar system. In *Protostars and planets II*, pages 1100–1153.

Johansen, A., Oishi, J. S., Low, M.-M. M., Klahr, H., Henning, T., and Youdin, A. (2007). Rapid plaentesimal formation in turbulent circumstellar disks. *Nature*, 448(30):1022–1025.

Kratter, K. M., Murray-Clay, R. A., and Youdin, A. N. (2010). The runts of the litter: Why planets formed through gravitational instability can only be failed binary stars. *The Astrophysical Journal*, 710(2):1375.

Levison, H. F., Morbidelli, A., Gomes, R., and Backman, D. (2007). Planet migration in planetesimal disks. *Protostars and planets V*, 1:669–684.

Lin, D. N. (2008). The genesis of planets. *Scientific American*, 298(5):50–59.

Lissauer, J. J. (1993). Planet formation. *Annual Review of Astronomy and Astrophysics*, 31(1):129–174.

Lissauer, J. J., Fabrycky, D. C., Ford, E. B., Borucki, W. J., Fressin, F., Marcy, G. W., Orosz, J. A., Rowe, J. F., Torres, G., Welsh, W. F., et al. (2011). A closely packed system of low-mass, low-density planets transiting kepler-11. *Nature*, 470(7332):53–58.

Matzner, C. D. and Levin, Y. (2005). Protostellar disks: formation, fragmentation, and the brown dwarf desert. *The Astrophysical Journal*, 628(2):817.

Mayor, M. and Queloz, D. (1995). A jupiter-mass companion to a solar-type star.

Noh, H., Vishniac, E. T., and Cochran, W. D. (1991). Gravitational instabilities in a protoplanetary disk. *The Astrophysical Journal*, 383:372–379.

Papaloizou, J. C. and Terquem, C. (2005). Planet formation and migration. *Reports on Progress in Physics*, 69(1):119.

Raymond, S. N. (2007). Terrestrial planet formation in extra-solar planetary systems. *Proceedings of the International Astronomical Union*, 3(S249):233–250.

Safronov, V. S. (1972). Evolution of the protoplanetary cloud and formation of the earth and planets. *Evolution of the protoplanetary cloud and formation of the earth and planets., by Safronov, VS. Translated from Russian. Jerusalem (Israel): Israel Program for Scientific Translations, Keter Publishing House, 212 p.*, 1.

Tanga, P., Weidenschilling, S., Michel, P., and Richardson, D. (2004). Gravitational instability and clustering in a disk of planetesimals. *Astronomy & Astrophysics*, 427(3):1105–1115.

Toomre, A. (1964). On the gravitational stability of a disk of stars. *The Astrophysical Journal*, 139:1217–1238.

Trilling, D. E., Lunine, J. I., and Benz, W. (2002). Orbital migration and the frequency of giant planet formation. *Astronomy & Astrophysics*, 394(1):241–251.

Watson, A. M., Stapelfeldt, K. R., Wood, K., and Ménard, F. (2007). Multi-wavelength imaging of young stellar object disks: Toward an understanding of disk structure and dust evolution. *arXiv preprint arXiv:0707.2608*.

Youdin, A. and Johansen, A. (2007). Protoplanetary disk turbulence driven by the streaming instability: linear evolution and numerical methods. *The Astrophysical Journal*, 662(1):613.

Youdin, A. N. (2003). Obstacles to the collisional growth of planetesimals. *arXiv preprint astro-ph/0311191*.

Youdin, A. N. and Goodman, J. (2005). Streaming instabilities in protoplanetary disks. *The Astrophysical Journal*, 620(1):459.

Youdin, A. N. and Shu, F. H. (2002). Planetesimal formation by gravitational instability. *The Astrophysical Journal*, 580(1):494.

Zuckerman, B. and Song, I. (2009). The minimum jeans mass, brown dwarf companion imf, and predictions for detection of y-type dwarfs. *Astronomy & Astrophysics*, 493(3):1149–1154.